The Company of Biologists

RESEARCH ARTICLE

The yeast *FIT2* homologs are necessary to maintain cellular proteostasis and membrane lipid homeostasis

Wei Sheng Yap[1],*, Peter Shyu, Jr[1],*, Maria Laura Gaspar[2], Stephen A. Jesch[2], Charlie Marvalim[1], William A. Prinz[3], Susan A. Henry[2] and Guillaume Thibault[1,4],‡

ABSTRACT

Lipid droplets (LDs) are implicated in conditions of lipid and protein dysregulation. The fat storage-inducing transmembrane (FIT; also known as FITM) family induces LD formation. Here, we establish a model system to study the role of the *Saccharomyces cerevisiae FIT* homologues (*ScFIT*), *SCS3* and *YFT2*, in the proteostasis and stress response pathways. While LD biogenesis and basal endoplasmic reticulum (ER) stress-induced unfolded protein response (UPR) remain unaltered in *ScFIT* mutants, *SCS3* was found to be essential for proper stress-induced UPR activation and for viability in the absence of the sole yeast UPR transducer *IRE1*. Owing to not having a functional UPR, cells with mutated *SCS3* exhibited an accumulation of triacylglycerol within the ER along with aberrant LD morphology, suggesting that there is a UPR-dependent compensatory mechanism that acts to mitigate lack of *SCS3*. Additionally, *SCS3* was necessary to maintain phospholipid homeostasis. Strikingly, global protein ubiquitylation and the turnover of both ER and cytoplasmic misfolded proteins is impaired in *ScFITΔ* cells, while a screen for interacting partners of Scs3 identifies components of the proteostatic machinery as putative targets. Together, our data support a model where ScFITs play an important role in lipid metabolism and proteostasis beyond their defined roles in LD biogenesis.

This article has an associated First Person interview with the first author of the paper.

KEY WORDS: Endoplasmic reticulum-associated degradation, ERAD, Lipid droplet, Proteostasis, Phospholipid metabolism, Scs3, Unfolded protein response, UPR

INTRODUCTION

Lipid droplets (LDs) have long been regarded as inert cytoplasmic organelles with the primary function of housing excess intracellular lipids. LDs arise from the endoplasmic reticulum (ER) and contain a core of the non-polar lipids triacylglycerol (TAG) and steryl ester (SE) surrounded by a phospholipid monolayer, with phosphatidylcholine (PC) as the major component (Grillitsch et al.,

2011). More recently, LDs have been strongly implicated in conditions of lipid and protein dysregulation. These conditions are major contributors to the pathophysiology of metabolic diseases and concomitantly activate cellular stress response pathways, namely the unfolded protein response (UPR) and heat-shock response (HSR). Increased LD biogenesis has been extensively observed in cells under stress conditions. Introduction of oxidative stressors or the attenuation of antioxidant capacities of cells result in the formation of LDs (Lee et al., 2013; Liu et al., 2015; Nguyen et al., 2017). While the extent of UPR activation and the resulting transcriptional profile differs between proteotoxic and lipid stress, a similar increase in lipogenic markers and concomitant LD formation is observed (Fei et al., 2009; Fun and Thibault, 2019; Ho et al., 2020; Hou et al., 2014; Lee et al., 2012; Thibault et al., 2012). It remains to be determined whether LDs contribute to stress induction or if this is reflective of the adaptive role of LDs to mitigate the otherwise deleterious effects of stress. However, all these undoubtedly highlight the complex integration of LDs in stress response pathways. In addition to this, the UPR regulates metabolic pathways to a certain extent under normal physiological conditions (Lee et al., 2008), and similarly orchestrates the complex transcriptional metabolic reprogramming under ER stress induction (Thibault et al., 2012).

The fat storage-inducing transmembrane (FIT; also known as FITM) family of proteins constitutes a group of evolutionarily conserved proteins eponymously named for their role in lipid metabolism and LD formation (Kadereit et al., 2008). In mammals, FIT proteins exhibit differential expression patterns, with FIT1 (FITM1) being expressed primarily in cardiac and skeletal muscle tissue, and FIT2 (FITM2) being more ubiquitously expressed. FIT proteins (FIT1/FIT2) are ER-resident proteins with a total of six transmembrane domains and with both N- and C- termini facing the cytosol (Gross et al., 2010; Kadereit et al., 2008). The *S. cerevisiae FIT2* homologs (*ScFIT*) *SCS3* and *YFT2* are predicted to share the same membrane topology. The pioneer study on the FIT proteins has identified their profound effect on the formation and accumulation of LDs both *in vitro* and *in vivo* (Kadereit et al., 2008). Transient overexpression of *FIT2* was sufficient to drive the formation of LDs, a process that was later hypothesized to be mediated by the capacity of FIT2 to directly bind and partition TAG from the ER into storage in LDs *in vitro* (Gross et al., 2010). Transgenic expression of the mammalian *FIT2* gene in the budding yeast *S. cerevisiae* (Moir et al., 2012) and in the plant models *Arabidopsis thaliana* and *Nicotiana tabacum* (Cai et al., 2017) induced the formation of cytoplasmic LDs. Similarly, transient expression of the *ScFIT* genes in mammalian cells *in vitro* led to the increased formation of LDs (Moir et al., 2012). A gain-of-function FIT2 mutant was identified with a 3-amino-acid mutation within its fourth transmembrane domain, which interestingly houses the most highly conserved amino acid residues from yeast to humans (Ramus et al., 2011). Conversely, it was found that the deletion of *FIT2*

[1]School of Biological Sciences Nanyang Technological University, Singapore, 637551. [2]Department of Molecular Biology and Genetics, Cornell University, Ithaca, NY 14853, USA. [3]Laboratory of Cell and Molecular Biology, National Institute of Diabetes and Digestive and Kidney Diseases, NIH, Bethesda, MD 20892, USA. [4]Institute of Molecular and Cell Biology, A*STAR, Singapore, 138673.
*These authors contributed equally to this work

‡Author for correspondence (thibault@ntu.edu.sg)

W.S.Y., 0000-0002-5411-2548; P.S., 0000-0003-2058-611X; W.A.P., 0000-0002-9053-2398; S.A.H., 0000-0002-2386-5184; G.T., 0000-0002-7926-4812

greatly compromised LD formation in the model organisms *Danio rerio* and *Caenorhabditis elegans*, as well as in the pathogenic yeast *Candida parapsilosis* (Choudhary et al., 2015; Kadereit et al., 2008; Nguyen et al., 2011). All these reports further reinforced the initial hypothesis of the FIT proteins directly functioning in LD biogenesis.

In contrast, *S. cerevisiae* deletion mutants for either or both *ScFIT* genes retain their capacity to form LDs, with size and number comparable to that in wild type (WT) (Moir et al., 2012). Upon closer investigation, it was found that LDs fail to completely bud off from the ER in the absence of the ScFIT proteins (Choudhary et al., 2015), presumably through alterations in ER membrane lipid properties (Choudhary et al., 2018). These findings have since then led to the investigation of alternative functions of the FIT class of proteins. *SCS3* was initially reported to have a putative role in the regulation of phospholipids (Hosaka et al., 1994), a function that was largely unexplored until a large-scale genetic screen reported on the strong interactions between the *ScFIT*s and genes involved in phospholipid biosynthesis, including *DGK1* and *PSD1* (Moir et al., 2012). In-depth analysis of the ScFIT protein sequences have since then revealed the presence of the catalytic site of a lipid phosphatase (Hayes et al., 2017). *In vitro* analyses have identified the capacity of mammalian FIT2 to hydrolyze phosphates from phosphatidic acid (PA) and lyso-PA to yield diacylglycerol (DAG) and monoacylglycerol (MAG), respectively. On the other hand, substrates for the lipid phosphatase activity of the ScFIT proteins have yet to be determined. This conserved catalytic function has been associated with the aberrant ER whorling phenotype observed in cells devoid of the FIT proteins (Hayes et al., 2017).

Conjointly, several different perspectives now exist on the function of the ScFIT proteins. However, definitive evidence for the function of FIT proteins in either binding and partitioning neutral lipids (NLs) or influencing NL and phospholipid metabolism in the complex *in vivo* environment remains scarce. Moreover, how any of these functions impact ER homeostasis and the UPR are partially unexplored.

In this study, we investigated the role of *SCS3*, identified as one of the downstream UPR target genes. As the UPR transducer Ire1 is essential for viability in the absence of *SCS3*, we generated the temperature-sensitive allele *scs3-1* to reveal its role without the masking effect of the UPR program. We demonstrated that dysfunctional *SCS3* leads to the accumulation of TAG at the ER, a shift in phospholipid distribution and the biogenesis of aberrant LD morphology. Furthermore, we identified the interactome of ScFITs, with Scs3 being found to interact with components of the proteostatic machinery. Next, we demonstrated that *ScFIT* mutants impaired the clearance of ER-associated degradation (ERAD) client proteins, which was exacerbated by lipid imbalance. Together, our data support a model where ScFITs play an important role in lipid metabolism and proteostasis beyond their defined roles in LD biogenesis.

RESULTS

Scs3 is essential for viability in the absence of UPR transducer Ire1

Previous synthetic genetic array (SGA) analyses have revealed the synthetic lethality between *SCS3* and *IRE1*, which encodes for the sole UPR transducer in yeast (Moir et al., 2012). Additionally, the mutant *scs3Δ* strain has been reported to activate the UPR (Jonikas et al., 2009), while *SCS3* has conversely been shown to be transcriptionally upregulated upon UPR activation resulting from either proteotoxic stress or lipid bilayer stress (LBS) (Ho et al., 2020; Thibault et al., 2012; Travers et al., 2000). As previously reported (Becuwe et al., 2020; Choudhary et al., 2015; Hayes et al., 2017), Scs3 and Yft2 proteins localize to the ER (Fig. S1A). Hence, we sought to further understand the role of *SCS3* within the UPR program. First, we monitored UPR activation using the UPR element (UPRE)-LacZ reporter assay (Cox and Walter, 1996). Unexpectedly, no significant UPR activation was observed in *scs3Δ* mutants, contradicting a previous report (Jonikas et al., 2009) while being consistent with other findings (Moir et al., 2012) (Fig. 1A). Similarly, there was no significant UPR activation in *yft2Δ* nor in *ScFITΔ* cells. All mutant strains were able to mount an UPR response upon treatment with the ER stress-inducing agent
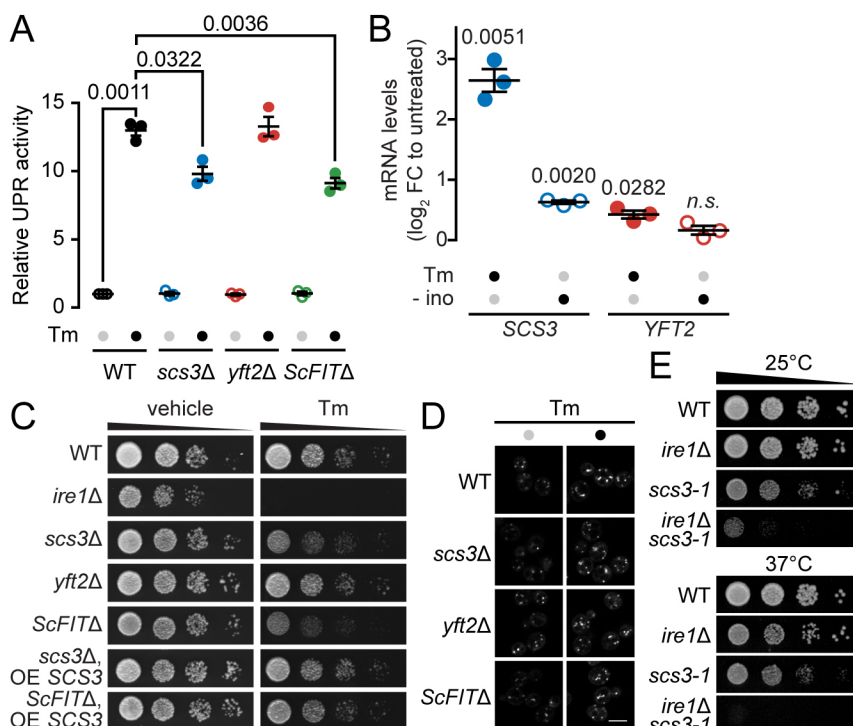
Fig. 1. Scs3 is essential for viability in the absence of UPR transducer Ire1. (A) Activation of the UPR was measured by a reporter assay utilizing the expression of the LacZ enzyme under the control of the *CYC1* promoter with the UPR element. Cells were either treated with the *N*-linked glycosylation inhibitor tunicamycin (Tm) or the carrier DMSO for 1 h prior to harvesting for the assay. (B) qPCR results comparing the mRNA levels of *SCS3* and *YFT2* in WT cells treated with 0.25 µg/ml tunicamycin (Tm) or in the absence of inositol (– ino), when indicated. (C) ScFIT mutant strains were grown in selective medium prior to dilution and spotting on vehicle or Tm-supplemented media. Culture plates were incubated at 30°C until colonies are observed. OE, overexpressed. (D) WT and *scs3Δ* mutant cells were treated with Tm for 1 h before LD staining with the fluorescent BODIPY 493/503 dye. Scale bar: 2 µm. Images shown are representative of three independent experiments. (E) Strains in the PER genetic background were grown at 25°C in minimal medium from which dilutions were prepared and spotted onto plates. Plates were incubated at the specified temperatures until colonies were observed. Data shown is the mean±s.e.m. from three independent experiments. Significant *P*-values are shown above graphs; *n.s.*, not significant (two-tailed Student's *t*-test). Gray dots are no treatment and black dots indicate the condition.

tunicamycin (Tm) although the level of activation was significantly lower in *scs3Δ* and *ScFITΔ*. Similarly, the heat-shock response (HSR), a cytosolic proteotoxic stress compensatory pathway, was dampened in *ScFITΔ* upon heat stress (Fig. S1B,C). To complement the UPR assay, we asked whether *SCS3* and *YFT2* genes are upregulated in a UPR-dependent manner. *SCS3* was significantly upregulated while *YFT2* was mildly upregulated in WT cells treated with Tm (Fig. 1B). As depleting the medium of inositol induces the UPR through LBS (Cox et al., 1997; Halbleib et al., 2017; Ho et al., 2020), we measured the mRNA levels of both genes upon inositol depletion (− ino) and only *SCS3* exhibited a mild, but significant, upregulation. To further assess the role of *SCS3* during ER stress, we carried out a growth assay. The spotting assay revealed that the lack of *SCS3* causes a growth defect in the presence of Tm which can be rescued with the overexpression (OE) of *SCS3* (Fig. 1C). Together, these results demonstrate that *SCS3* is essential during ER stress conditions.

As lipogenic pathways constitute one of the major effectors of the UPR (Cretenet et al., 2010) and LDs are associated with stress conditions, the putative function of Scs3 in LD formation might then provide a rationale for its UPR-dependent transcriptional upregulation. We further hypothesized that the inability of *scs3Δ* mutants to mount a maximal UPR under proteotoxic stress conditions may translate to the impairment of LD formation as part of the stress response. We made use of fluorescent BODIPY 493/503 to stain LDs in *scs3Δ* mutants challenged with Tm-induced stress to evaluate gross changes in LD formation. The mutant cells were still able to form LDs to the same extent as WT cells under unstressed and ER stressed conditions (Fig. 1D, Fig. S1D). Next, we sought to determine the extent by which the UPR compensates for the absence of *SCS3*, particularly in respect to LD formation. However, a *scs3Δire1Δ* mutant is synthetically lethal, thus rendering conventional deletion strategies unusable in titrating the phenotypic effects of the UPR upon the loss of *SCS3*. To address this, we generated a conditional temperature-sensitive *scs3* allele (*scs3-1*) that is functional at a permissive temperature of 25°C but not at the restrictive temperature of 37°C (Fig. 1E, Fig. S2), using a screening strategy that we previously reported (Thibault et al., 2011, 2012; Thibault and Ng, 2011). As *IRE1* is not essential in the absence of *YFT2* (Fig. S2B), a temperature-sensitive allele of *YFT2* was not needed. This provides strong support for the interdependence between *IRE1* and *SCS3*, and that each is required for viability in the absence of the other, consistent with SGA results showing synthetic lethality between these two genes (Moir et al., 2012).

Scs3 is essential for the maintenance lipid homeostasis at the ER and LD morphology
In *scs3Δ* and *yft2Δ* mutants, LDs remain irreversibly tethered to the ER and are wrapped by a membrane. Jacquier et al. suggest that, in yeast, LDs always remain connected to the ER (Jacquier et al., 2011). We hypothesized that while the knockout strains we used are fully capable of forming LDs (Fig. 1D), it is possible that these LDs remain tightly integrated in the ER membrane, resulting in the disruption of ER lipid homeostasis, as previously reported (Choudhary et al., 2018, 2015). Strains with temperature-sensitive alleles were grown to early log-phase at 25°C followed by a temperature shift of 2 h at 37°C. To assess the levels of neutral lipids in the ER, we extracted total lipids from microsomes of the cells, and TAGs were separated by thin layer chromatography (TLC) and quantified by gas chromatography with a flame ionization detector (GC-FID) (Fig. 2A; Fig. S3). A significant increase in TAGs within the microsomal fractions of *scs3-1* strain was only observed in the

absence of *IRE1* at the restrictive temperature of 37°C, thereby suggesting that the presence of the UPR exerts a suppressive effect for this phenotype. As it has been previously shown that LDs are wrapped with ER membranes in *scs3Δ* and *yft2Δ* yeast mutants using the inducible TAG synthesis system (Choudhary et al., 2015), we asked whether the UPR plays a role in the budding and morphology of LDs. Transmission electron microscopy (TEM) was performed on *scs3-1* and *ire1Δscs3-1* cells following a temperature shift. Strikingly, we observed irregular LD morphology in *scs3-1* and *ire1Δscs3-1* cells (Fig. 2B; Fig. S4). The abnormally elongated LDs were embedded in ER. Additionally, LDs were smaller in *ire1Δscs3-1* cells compared to those in *scs3-1* cells at 37°C. Taken together, our findings suggest that Scs3 is necessary for LDs to form on the exoleaflet of the ER and that the UPR plays an important role in regulating TAG levels.

The transcription of a subset of genes encoding phospholipid biosynthesis enzymes are inhibited in the presence of phospholipid precursors inositol and choline (Carman and Henry, 1999; Carman and Kersting, 2004; Henry and Patton-Vogt, 1998). Additionally, the absence of inositol in yeast growth medium induces the UPR (Cox et al., 1997; Halbleib et al., 2017; Ho et al., 2020). Therefore, we asked whether Scs3 plays a role in modulating phospholipid homeostasis in the absence of inositol and choline. We performed lipid analysis of cells grown in medium containing inositol and choline to mid-logarithmic phase before being shifted to a 3 h incubation in medium lacking inositol and choline. Unexpectedly, *scs3Δ* mutant cells contained four times the phosphatidylcholine (PC) levels of WT cells (Fig. 2C). We also tested *scs3Δ pct1Δ* cells because Pct1 is a cholinephosphate cytidylyltransferase enzyme, so these cells are unable to synthesize PC from the precursor choline through the Kennedy pathway. PC levels of *scs3Δ* cells were significantly decreased in the *pct1Δ* background mutant, suggesting that PC is mostly synthesized through the Kennedy pathway in the absence of *SCS3*. Phosphatidylserine (PS) and phosphatidylethanolamine (PE) were also found to be two times more abundant in *scs3Δ* mutant compared to WT cells, while there was no significant difference in phosphatidylinositol (PI) levels. Next, we tested whether supplementing the medium with inositol and choline would restore phospholipid levels in the *scs3Δ* mutant. In contrast to what was found in the absence of both lipid precursors, we observed a decrease of about four times of PC in the *scs3Δ* mutant compared to WT cells (Fig. 2D). There was also a significant decrease of PI in the *scs3Δ* mutant. To further understand the role of Scs3 in modulating phospholipids, we measured the levels of PC and PI over the course of 3 h of cells grown in media depleted of inositol followed by a 0.5 h recovery (+ ino) period. In the presence of choline, *scs3Δ* cells failed to increase the synthesis of PI upon the re-introduction of inositol while PI level increased rapidly in WT (Fig. 2E). On the other hand, there was a constant decrease of PC levels in *scs3Δ* while PC levels continually increased in WT during the 3 h of inositol depletion. Together, these data reveal that Scs3 is essential to maintain phospholipid homeostasis. We speculate that the decrease of PI in *scs3Δ* cells might alter the composition of complex sphingolipids (Guan et al., 2009), which in turn would induce the UPR (Liu et al., 2012).

Scs3 interacts with components of the proteostatic machinery
To gain further insight into the physiological relevance of ScFIT proteins within the cell, we employed the split-ubiquitin-based membrane yeast two hybrid (MYTH) screen (Snider et al., 2010). The reporter moiety was fused to the N-terminal or the C-terminal cytosolic domains of both Scs3 and Yft2. The four bait constructs
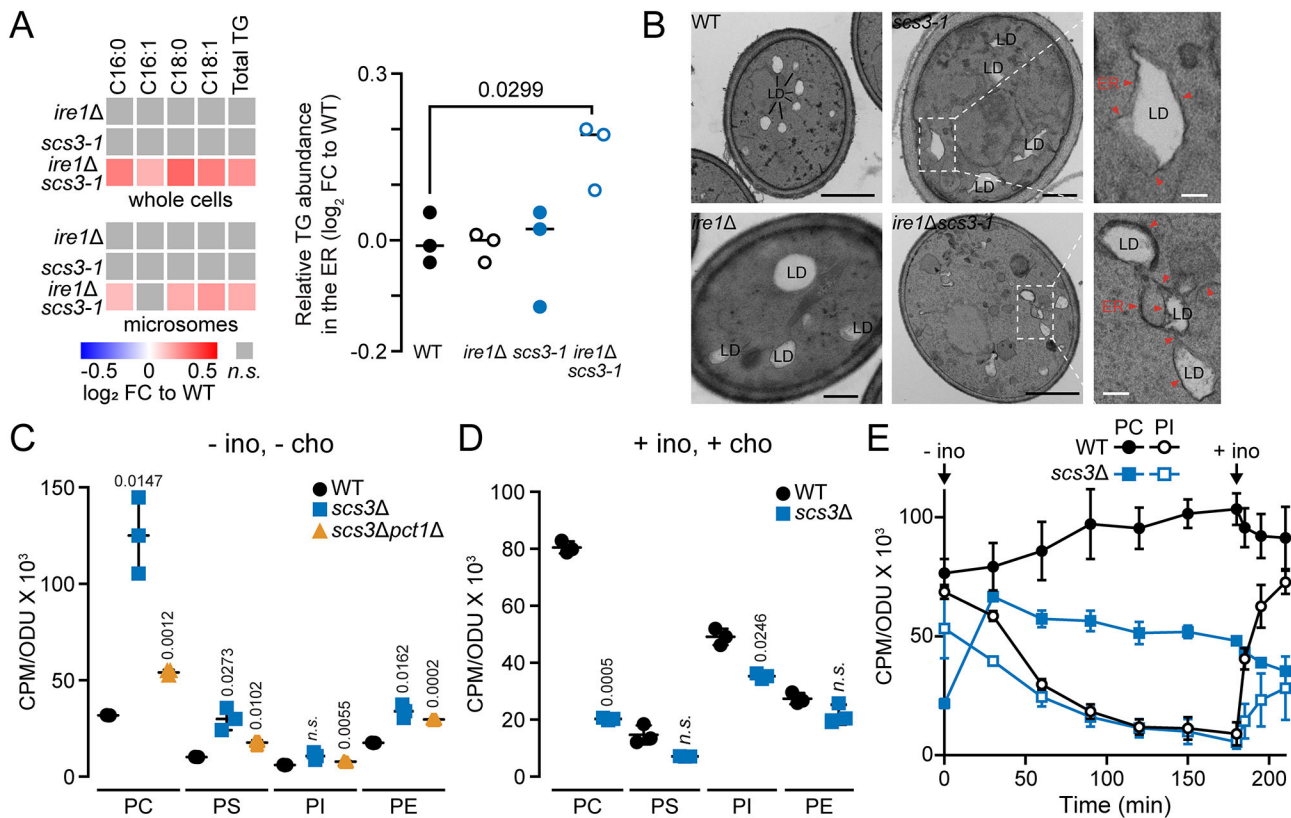
Fig. 2. Scs3 is necessary to maintain lipid homeostasis and LD morphology. (A) Strains were grown to log phase at 25°C in minimal medium, after which the temperature was shifted to 37°C for 2 h. Lipids were extracted from whole cells or from isolated microsomes, and separated on TLC plates. All fatty acid (FA) species derived from TAG (labeled TG) were normalized against WT levels. Relative TAG abundance was determined by FAME analysis through GC-FID and normalized against WT. (B) Strains were grown to log phase at 25°C in minimal medium and shifted to 37°C for 2 h before imaging by TEM. Scale bars: 500 nm (main images); 100 nm (magnified views). ER, endoplasmic reticulum; LD, lipid droplet. (C) Phospholipid levels of cells grown in medium without inositol and choline (− ino,−cho) in the presence of [^{32}P]orthophosphate. Phosphatidylcholine (PC), phosphatidylserine (PS), phosphatidylinositol (PI) and phosphatidylethanolamine (PE) were separated by thin layer chromatography (TLC). (D) Phospholipid levels of cells grown in medium with inositol and choline (+ ino, +cho) treated as in C. (E) PC and PI levels of cells transferred to media depleted of inositol (− ino) but with choline over the course of 3 h followed by a reintroduction of inositol (+ ino) for a period of 0.5 h. Data shown is the mean±s.e.m. from three independent experiments. Significant P-values are shown above graphs; n.s., not significant (two-tailed Student's t-test).

were validated, and screening conditions for each were optimized with 3′-amino-1,2,4,-triazole (3′-AT) supplementation in the selection medium to reduce the occurrence of false positives. Following this, 1344 colonies were collectively screened for all reporter strains. From these, 664 colonies were positive for bait–prey interaction as manifested by blue colony growth on 5-bromo-4-chloro-3-indolyl-β-D-galactopyranoside (X-gal)-supplemented selective medium and were designated as putative interactors (Fig. S5). These were further validated for specificity towards the bait protein of interest in comparison to the single-pass human cluster of differentiation 4 (CD4) receptor protein, which served as a negative control. From these, 189 showed specific interactions with the ScFIT proteins. Following sequence analysis, 88 unique protein interactors were identified. Considering the overlap in protein interactors, the MYTH screen identified a total of 73 genuine and unique interactors for the ScFIT proteins, which were further categorized according to cellular functions (Fig. 3). Moreover, our screen results show that more than half of the identified Yft2 protein interactors are shared with those of Scs3, thereby supporting a certain degree of functional redundancy between the two proteins.

Surprisingly, only few of the ScFIT protein interactors identified with the screen are directly involved in lipid metabolism, suggesting that ScFIT proteins may not function extensively in that cellular process. It should also be noted that, while the encoded proteins of

genes that ScFIT had high degrees of genetic interactions with, such as ICE2, SEY1 and UBX2 (Moir et al., 2012; Tavassoli et al., 2013), were not identified with the MYTH screen, this does not exclude the possibility of a physical interaction. However, our results alternatively suggest that, despite having a high degree of genetic interaction, these proteins function in parallel but independently in the same cellular process, and that the loss of both is detrimental to cell viability.

Interestingly, several proteins that function in proteostasis and the ubiquitin-proteasome system (UPS) have been found to interact with Scs3 (Fig. 3, Fig. S5). Of note are the J-protein chaperone Zuo1 and the Hsp70 chaperone Ssb2, both of which have been reported to function in protein quality control (Allen et al., 2007; Chiabudini et al., 2012; Ohba, 1994). Doa10 is one of the key E3 ubiquitin ligases in yeast, and is involved in ER-associated degradation (ERAD) of proteins (Habeck et al., 2015; Ravid et al., 2006; Swanson et al., 2001). Taken together, these results suggest that Scs3 may function to a certain extent in protein quality control pathways, specifically in the UPS.

The clearance of ERAD client proteins is impaired in ScFIT mutants
As the accumulation of misfolded proteins and the ensuing proteotoxicity is closely related to the ability of cells to efficiently
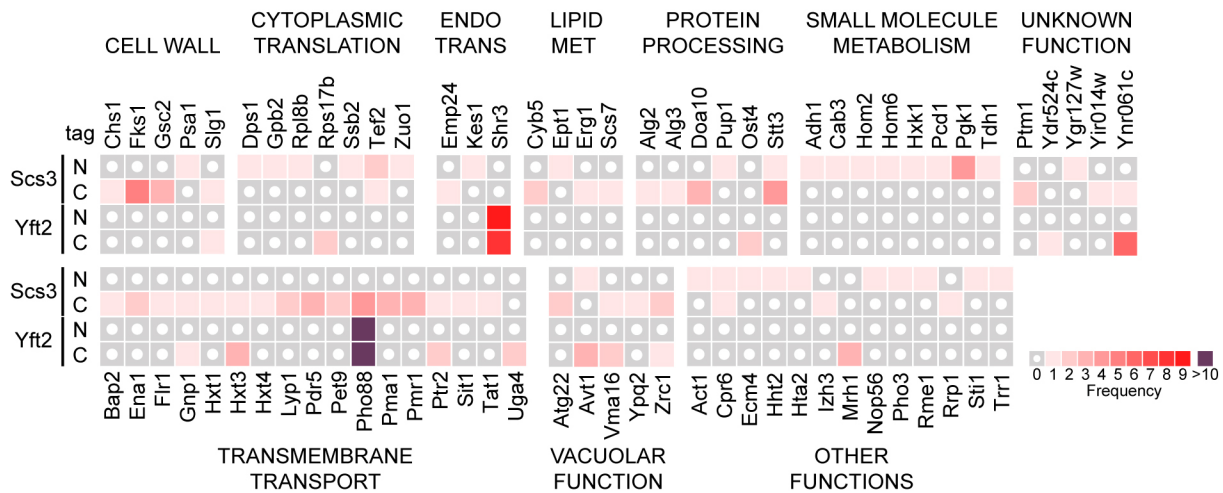
Fig. 3. The ScFIT interactome as identified by membrane yeast two-hybrid screening. The frequency by which each unique protein interactor was identified in ScFIT reporter constructs tagged in either N or C-terminus is represented in a heat map and are grouped according to function.

process client proteins, we hypothesized that the sensitivity to Tm exhibited by *scs3Δ* and *ScFITΔ* mutants may be the result of impaired protein degradation pathways, as in the case of *ubx2Δ* mutants, which have impaired turnover of both misfolded ER and cytosolic substrates (Spear and Ng, 2003). Following the identification of UPS machinery components as protein interactors of Scs3, we asked whether ScFIT proteins play a role in protein ubiquitylation. We overexpressed Myc-tagged ubiquitin (Ub-Myc) through the inducible *CUP1* promoter and quantified the extent of total protein ubiquitylation in cells by immunoblotting. The amount of ubiquitylated proteins in *ScFITΔ* mutants was significantly reduced, by ∼38%, relative to that of WT cells, with a less-pronounced reduction of 18% in *scs3Δ* single mutants (Fig. S6A). Since the stabilization of protein substrates was accompanied by a decrease, rather than an increase in high molecular mass ubiquitin antibody-reactive proteins, the inefficient turnover of the said substrates is likely due to a failure to mark them correctly for degradation and not because of efficient clearance in the proteasome.

To investigate whether the global decrease of ubiquitylated proteins correlates with protein stability, we measured the turnover of known ERAD substrates in ScFIT mutants by means of a cycloheximide chase assay. We expressed HA-tagged Sbh2, Yeh1 and Pgc1 in *ScFITΔ* mutants. These native proteins are dependent on Doa10-mediated ERAD for normal degradation (Habeck et al., 2015; Ruggiano et al., 2016). The turnover rates of Sbh2 and Yeh1 in *ScFITΔ* mutants was similar to that of WT (Fig. S6B,C). In contrast, the degradation of Pgc1 was significantly accelerated in *ScFITΔ* mutants (Fig. S6D). Along with the identification of Pgc1 as a Doa10-dependent ERAD substrate, its proper localization dynamics between the ER and LD membranes was found to be critical in determining its stability (Ruggiano et al., 2016). Doa10 reportedly recognizes ER-localised Pgc1 through its hairpin loop, which then serves as a degron that concentrates Pgc1 on the surface of LDs. As LDs fail to properly mature in the absence of the ScFIT proteins (Fig. 2B), the lateral diffusion of the pool of Pgc1 proteins to the ER may be increased in *ScFITΔ* mutants, resulting in continual degradation by Doa10 (Kory et al., 2016). We hypothesized that native proteins in their proper conformation, like Pgc1, may not illicit a proteotoxic effect on *ScFITΔ* cells, and that an otherwise compromised protein degradation pathway in this mutant could remain fully capable of clearing these endogenous proteins.

As misfolded model substrate, we monitored the protein levels of epitope-tagged versions of misfolded CPY (CPY*–HA) (Fig. 4A). A small but significant delay in the degradation of CPY* was only observed in *ScFITΔ* mutants and not in *scs3Δ* nor *yft2Δ*. Next, we measured the degradation rates of the engineered misfolded variant of the Pep4 vacuolar protease (ngPrA*Δ295-331–HA) (Kanehara et al., 2010) (Fig. 4B). In contrast to CPY*, *ScFITΔ* cells exhibited a strong defect in the degradation of ngPrA*Δ295-331–HA in comparisons to WT and single mutants. Both CPY*–HA and ngPrA*Δ295-331–HA are luminal soluble substrates, which are degraded in a Hrd1-dependent manner (Kanehara et al., 2010; Thibault et al., 2011). To further assess whether the global decrease of ubiquitylated proteins is associated with ScFIT, we monitored the degradation of San1-dependent cytosolic protein quality control (CytoQC) substrates Δ2GFP–HA and ssPrA–HA (Prasad et al., 2010). Consistent with our results using misfolded ERAD substrates, we found that *ScFITΔ* mutants are unable to efficiently clear away both cytosolic substrates compared to WT cells or either of the single mutants (Fig. S6E,F). As neither of the single deletion mutants resulted in a stabilization of the ERAD substrates, the two proteins may share a redundant yet poorly understood function. *YFT2* is reported to have been the result of the segmental duplication of *SCS3* (Moir et al., 2012). This is supported by the more-pronounced growth sensitivity to Tm in the double *ScFITΔ* mutant in comparison to a mild defect in *scs3Δ* cells (Fig. 1C). This, along with the broader range of Scs3 protein interactors (Fig. 3), also suggests an asymmetric redundancy wherein *YFT2* only partially compensates for the absence of *SCS3* functionality in the ERAD pathway, which ultimately results in less-apparent phenotypic defects in *yft2Δ* mutants.

To further investigate the role of lipid homeostasis and protein quality control, we monitored the degradation of CPY* in *ScFITΔ* mutant strains supplemented with inositol (+ino, −cho), choline (−ino, +cho), or both (+ino, +cho). There was a significant defect in the degradation of CPY* in *scs3Δ* and *yft2Δ* supplemented with choline compared to inositol (Fig. 4C,D). Similarly, the degradation of CPY* was slower in *scs3Δ* and *ScFITΔ* compared to WT in the presence of choline. Next, to validate the role of Scs3 in modulating ERAD, we monitored the degradation of ngPrA*Δ295-331–HA in *ScFITΔ* cells overexpressing (OE) *SCS3*. In *ScFITΔ*, ngPrA*Δ295-331–HA was degraded at a significantly slower rate than in WT cells
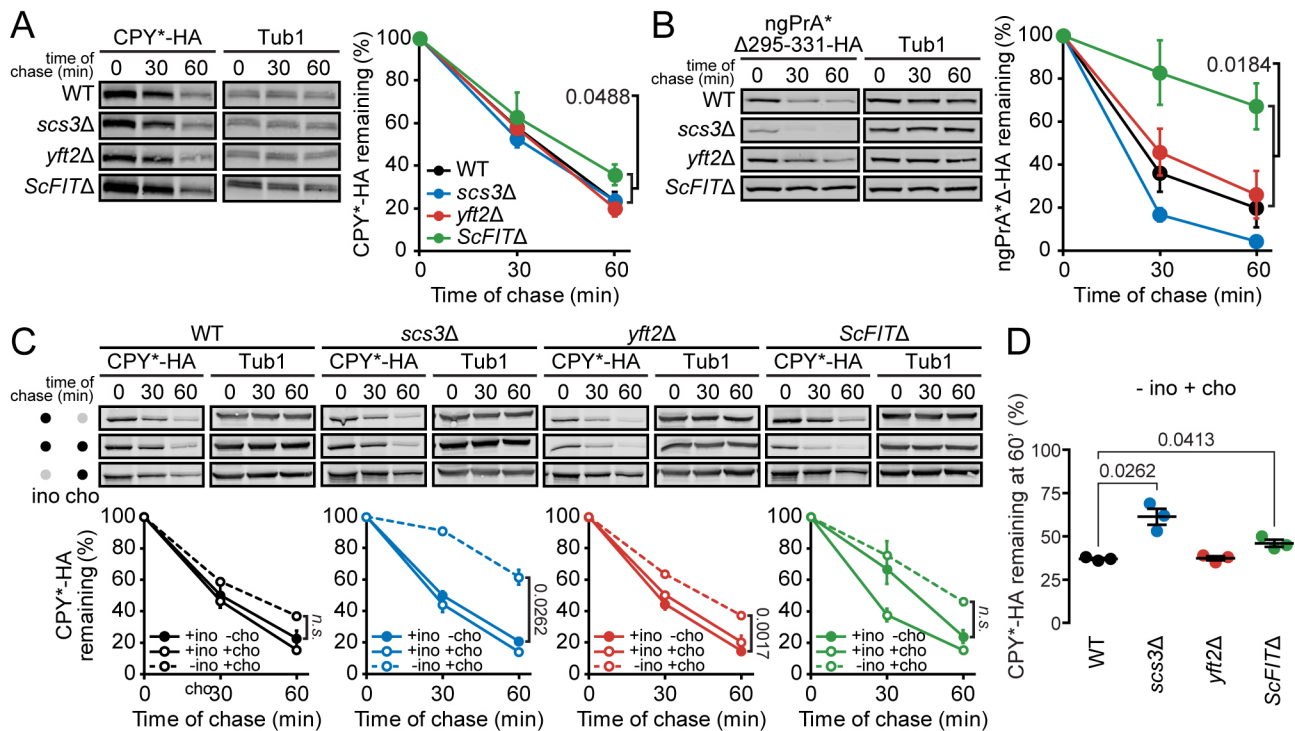
Fig. 4. The clearance of ERAD client proteins is impaired in *ScFIT* mutants. (A,B) Protein levels of the model Hrd1-dependent ERAD substrates (A) CPY*–HA and (B) ngPrA*Δ295-331–HA, were monitored at 0, 30 and 60 min time points following the attenuation of protein translation through treatment with cycloheximide. (C) Strains were treated as in A but were grown in the presence of inositol and absence of choline (+ ino,−cho), in the presence of inositol and choline (+ ino,+cho), or in the presence of choline and absence of inositol (− ino,+cho). Gray dots indicate not present and black dots indicate presence. (D) Percentage of CPY*–HA remaining at 60 min of samples grown in the presence of choline and absence of inositol (− ino,+cho). Data shown are the mean±s.e.m. from three independent experiments. Significant *P*-values are shown above graphs (two-tailed Student's *t*-test).

(Fig. 5A). On the other hand, the degradation of ngPrA*Δ295-331–HA was similar in *ScFITΔ* OE *SCS3* to WT and *ScFITΔ* strains, suggesting that *SCS3* is sufficient to rescue the ERAD defect. In the presence of choline (− ino,+cho), the degradation of ngPrA*Δ295-331–HA was decelerated in the three strains (Fig. 5B). Interestingly, OE *SCS3* in *ScFITΔ* cells supplemented with choline (− ino,+cho) significantly accelerated the degradation of CPY*-HA compared to WT and *ScFITΔ* (Fig. 5C). As lipid homeostasis correlates with ERAD fitness (Shyu et al., 2019; Thibault et al., 2012), these findings reinforce the notion that ScFIT is essential to regulate lipid levels at the ER and that these proteins contribute to ER proteostasis.

DISCUSSION

LDs have been increasingly implicated in disease pathophysiology. Despite this, our understanding of their involvement is obscure at best, as LD biology is still in its infancy, and more mechanistic insight into LD formation is warranted to grasp its relevance and importance in physiological processes. From the simple budding yeast, several proteins have been identified to influence LD generation (Adeyo et al., 2011; Cartwright et al., 2015; Szymanski et al., 2007). Among these, the FIT2 class of proteins has gained much interest in recent years, but its initial putative role in LD formation as a lipid-binding protein has recently been contested in favor of a broader function in membrane homeostasis. However seemingly disparate, the identification of lipid phosphatase activity in FIT2 may not be mutually exclusive with previous reports of its involvement in LD biogenesis. Given this, the molecular mechanism by which these two processes are linked is poorly understood, as well as the potential implication of FIT2 in normal functioning of cells outside the context of LD formation. In

this study, we report on the involvement of the yeast FIT homologs (ScFIT) not only in the maintenance of ER membrane homeostasis, but also in coordinating the cellular stress response pathway, namely the UPR, and the consequent impact on protein quality control (Fig. 6).

The complexity of lipid metabolic pathways is underscored by the highly interconnected conversion of intermediates as well as the various organelles and proteins that mediate these processes (Henry et al., 2012; Klug and Daum, 2014). In addition to this, perturbation of the lipid metabolic pathways results in the extensive reprogramming of the bioenergetic network (Natter and Kohlwein, 2013; Stordeur et al., 2014). Similarly, cellular insults also alter the lipidomic landscape of cells, suggestive of the buffering capacity of lipid pathways against stress conditions. Proteotoxic or LBS both activate the UPR and similarly culminate in the formation of LDs. Interestingly, none of the previously reported major protein effectors of LD biogenesis were identified as UPR targets. Moreover, apart from the SE biosynthetic *ARE2*, no other NL synthesis players are upregulated under conditions of ER stress (Thibault et al., 2012; Travers et al., 2000). Therefore, Scs3 upregulation under the UPR program could be part of the effort to orchestrate membrane remodeling.

It was reported that LDs in *ScFITΔ* cells remain embedded in the ER due to the enrichment of DAG, a lipid species with negative membrane curvature, as is the case with the accumulation of PE in a mutant of *CHO2*, a methyltransferase for PC synthesis (Choudhary et al., 2018). Interestingly, the addition of either of the positive curvature phospholipids, lyso-PC or lyso-PA, rescued the aberrant LD budding of *ScFITΔ* cells. The failure of the UPR to restore proper LD maturation in *cho2Δ* cells may result from the markedly
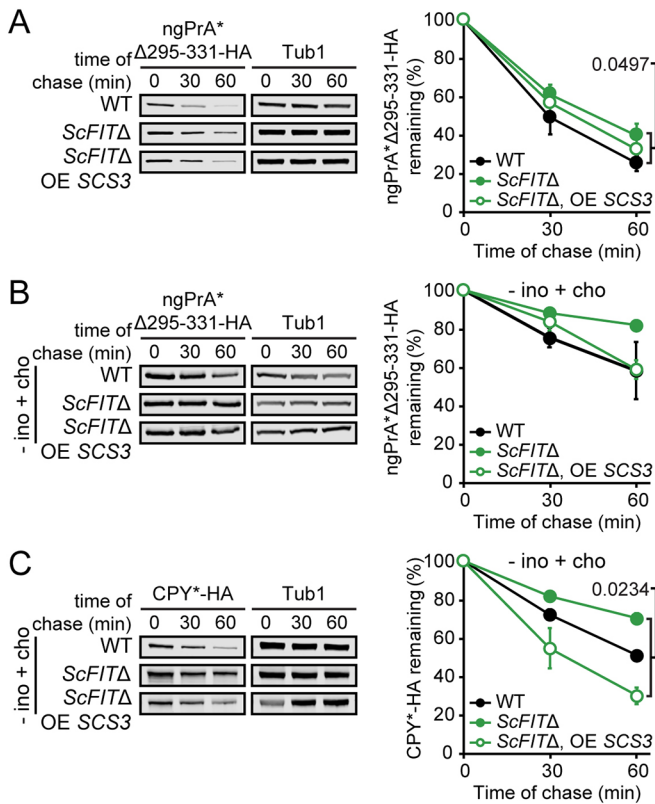
**Fig. 5. Scs3 is sufficient to rescue proteostatic defect of *ScFITΔ*.**
(A) ngPrA*Δ295-331–HA protein levels were monitored at 0, 30 and 60 min time points following the attenuation of protein translation with cycloheximide. OE, overexpressed. (B) ngPrA*Δ295-331–HA protein levels in cells treated as in A but in the absence of inositol (– ino,+cho). (C) CPY*–HA protein levels of cells treated as in A but in the absence of inositol (– ino,+cho). Data shown are the mean±s.e.m. from three independent experiments. Significant *P*-values are shown above graphs (two-tailed Student's *t*-test).

reduced capacity to synthesize PC, which exhibits a neutral curvature and is an intermediate to lyso-PC (van Meer et al., 2008). While *cho2Δ* cells indeed accumulated high levels of PE, DAG levels are dramatically reduced (Thibault et al., 2012). This, taken together with the observation that the gain-of-function DAG-binding FIT mutant failed to rescue the aberrant ER membrane whorling in *scs3Δ* cells (Becuwe et al., 2020), strongly suggests that the defects in ER membrane properties that lead to impaired LD maturation are independent of DAG. In contrast, we observed an accumulation of TAG at the ER, together with irregularly shaped LDs that were detached to the ER in *scs3-1* (Fig. 2B; Fig. S4), reinforcing the idea that Scs3 has a role in lipid homeostasis. While the catalytic activity of mammalian FIT2 on PA and lyso-PA was not identified in ScFIT proteins (Hayes et al., 2017), this does not

exclude the possibility that the latter may instead act on other membrane lipid species *in vivo*. In a recent paper, mammalian FIT2 is proposed to be a lipid phosphate phosphatase enzyme based on *in vitro* evidence (Becuwe et al., 2020). As *SCS3* is essential for viability in the absence of a functional UPR (Fig. 1), it can then be hypothesized that Scs3 regulates ER membrane lipid composition. Taken together, these findings highlight the important role of Scs3 in maintaining ER lipid homeostasis beyond LD biogenesis. A unifying model on the role of Scs3 *in vivo* with it acting as an enzyme that catalyzes lipid synthesis, regulates other enzymes or regulates lipid metabolism through other ways should emerge in future studies.

The loss of both FIT homologs in *ScFITΔ* mutants led to the unexpected stabilization of misfolded proteins in both within the ER and in the cytoplasm (Figs 4 and 5; Fig. S6E,F), which correlated with a global decrease in protein ubiquitylation (Fig. S6A). The maintenance of ER membrane integrity and lipid homeostasis are critical in supporting organellar function. Loss of *ICE2* causes altered ER membrane dynamics, including defects in mother–daughter cell ER membrane inheritance and ER–plasma membrane tethering (Estrada de Martin et al., 2005; Loewen et al., 2007). This ER membrane perturbation further impaired cellular functions, such as phospholipid regulation and protein degradation (Markgraf et al., 2014; Quon et al., 2018; Schuldiner et al., 2005; Tavassoli et al., 2013). Similarly, mutants of the phospholipase Lpl1, which catalyzes the turnover of phospholipids, also exhibited ERAD defects (Selvaraju et al., 2014; Weisshaar et al., 2017). The general disruption of lipid metabolism by attenuating fatty acid synthesis in turn caused defects in processing of ERAD client proteins in mammalian systems (To et al., 2017), which may also be in part due to its indirect effects on membrane lipid composition. Conversely, defective protein turnover also exerted a direct effect on membrane composition. The deletion of the ERAD component *UBX2* led to severe changes in ER membrane morphology due to dysregulation of Mga2 processing and the subsequent expression of its transcriptional target *OLE1*, a key regulator of membrane lipid saturation (Surma et al., 2013). Sterol content within membranes is also under tight control by protein quality control pathways, as the key enzymes Hmg2 and Erg1 are regulated in an ERAD-dependent mechanism (Foresti et al., 2013; Hampton et al., 1996). Intriguingly, these mutants have aberrant membranes and exhibit impaired LD formation in addition to curtailed protein turnover (Markgraf et al., 2014; Wang and Kaufman, 2012; Weisshaar et al., 2017).

In a previous study, we have shown that the singular UPR transducer Ire1 in yeast is strongly activated upon genetic alterations of ER membrane composition (Thibault et al., 2012). We also identified a LBS-sensing switch located at the interface of the amphipathic and transmembrane helices (Ho et al., 2020) while key residues within the amphipathic helix of Ire1 were reported to be important to sense LBS- and proteotoxic-induced ER stress
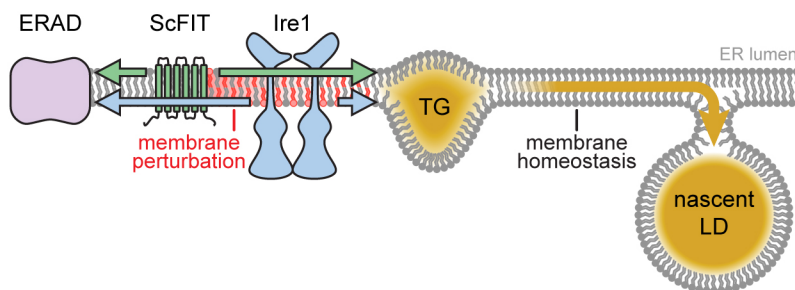
Fig. 6. Model for the putative role of ScFIT proteins in coordinating lipid and protein homeostasis. Both ScFIT and Ire1 proteins play a role in membrane homeostasis by preventing aberrant TAG (TG) accumulation within the ER, thereby contributing to LD maturation. Additionally, ScFIT and Ire1 proteins modulate the proteostatic ERAD pathway.

(Halbleib et al., 2017). As ER membrane morphology is compromised in ScFIT mutants, it could be hypothesized that proper Ire1 and UPR activation may not proceed as efficiently, which in turn affects ERAD function. In line with this, several studies lend support for the modulation of LDs by protein quality control pathways including ERAD. The *ubi4Δ* mutant was reported to exhibit less LD accumulation compared to that of WT cells under stress (Ishii et al., 2018). While the rationale for this increase in LD remains enigmatic, it suggests that LD formation may in part be regulated by ubiquitylation processes. This agrees with previous studies that detailed on the dependence of the NL biosynthetic enzyme Dga1 and SE lipase Yeh1 on Doa10 for their endogenous turnover (Ruggiano et al., 2016), and that the recruitment of the mammalian ERAD factor UBXD8 onto the LD surface regulates LD growth by modulating lipolysis (Olzmann et al., 2013). Apart from LDs, ERAD pathways also regulate the ER membrane composition and phospholipid turnover. The Cdc48 ATPase mediates the processing of the ER membrane sensors Mga2 and Spt24, to yield the cognate transcription factor for *OLE1* regulation (Kandasamy et al., 2004; Shcherbik and Haines, 2007; Surma et al., 2013), and the degradation of phosphorylation-inactive Pah1 is impaired in proteasome and ubiquitylation mutants (Hsieh et al., 2015; Pascual et al., 2014). Taken together, these greatly emphasize the interdependence of membrane homeostasis and protein quality control pathways.

In this study, we build on the current hypothesis on the role of ScFIT proteins in LD formation and membrane homeostasis, and further provide support for its functioning in cell stress response pathways to exert effects on these two processes (Fig. 6).

MATERIALS AND METHODS

Strains and antibodies

Saccharomyces cerevisiae strains used in this study are listed in Table S1. Strains were generated using standard cloning protocols. Anti-HA mouse monoclonal antibody HA.11 (1:2000; Covance MMS-101R-1000), anti-tubulin mouse monoclonal antibody 12G10 (1:10,000; DHSB), and anti-Myc mouse monoclonal antibody (1:5000; Invitrogen R950-25), were commercially purchased. Secondary antibodies goat anti-mouse IgG-DyLight 488 (Thermo Fisher 35503, Waltham, MA), goat anti-mouse IgG-IRDye 800 (LI-COR Biosciences 926-32210) and goat anti-rabbit IgG-IRDye 680 (LI-COR Biosciences 926-68021) were commercially purchased.

Plasmids used in this study

Plasmids and oligonucleotide primers used in this study are detailed in Tables S2 and S3, respectively. Plasmid constructs were generated through either conventional restriction enzyme cloning methods or Gibson assembly (New England Biolabs). The mutant *scs3* library was generated by low-fidelity PCR using primers PS1 and PS2 to amplify the promoter, coding sequence and terminator regions of the *SCS3* from the genomic DNA of wild-type (WT) cells. The PCR product was then digested with the enzymes *EcoRI* and *XbaI* before ligation into pGT0004. Plasmid pGT0364 was obtained through a colony sectoring screen detailed in the 'Genetic screen for temperature sensitive alleles' section below. Plasmid pGT0286, encoding for WT *SCS3*, was similarly generated using conventional PCR amplification. To generate reporter constructs for the membrane yeast two-hybrid screen, the coding sequences of *SCS3* and *YFT2* were amplified from WT yeast DNA using primer pairs PS39- and PS40, and PS159 and PS160, respectively. These were then inserted via Gibson assembly into vector backbones generated through PCR from pGT0317 using primer pairs PS39 and PS40, and PS157 and PS158, respectively, to generate pGT0374 and pGT0427. Plasmids pGT0426 and pGT0428 were generated through Gibson assembly by amplifying the coding sequence of *SCS3* and *YFT2*, terminating immediately before the stop codon using WT yeast DNA with primer pairs PS107 and PS108, and PS101 and PS102, respectively. These were then cloned into PCR-amplified vector backbones using pGT0318 as

template with primer pairs PS105 and PS106, and PS36 and PS99, respectively.

Spotting growth assay

Strains were grown to saturation in appropriate selective medium overnight at 30°C (or at 25°C for the temperature sensitive strains). Cultures were diluted to 0.2 OD_{600}/ml and serially diluted five-fold for a total of four dilutions. The cell suspensions were then spotted onto appropriate agar plates and incubated at indicated temperatures until the appearance of colonies.

β-galactosidase reporter assay

The β-galactosidase reporter assay was carried out as previously described (Thibault et al., 2011). Typically, cells were grown to early log phase, and tunicamycin (Tm) was added to growth cultures when specified at a concentration of 2.5 μg/ml to cells 1 h prior to harvest or a temperature shift to 37°C, for the induction of the UPR and HSR, respectively. Four OD_{600} units of cells were pelleted, washed and resuspended in 75 μl LacZ buffer (125 mM sodium phosphate pH 7, 10 mM KCl, 1 mM MgSO₄, 50 mM β-mercaptoethanol). An aliquot of 25 μl was transferred into 975 μl ddH₂O and the absorbance was measured at 600 nm. To the remaining suspension, 50 μl of CHCl₃ and 20 μl of 0.1% SDS were added and vortexed vigorously for 20 s. The reaction was started with the addition of 700 μl of 2 mg/ml 2-nitrophenyl-β-galactopyranoside (ONPG; Sigma) in LacZ buffer. Next, the reaction was quenched with 500 μl of 1 M Na₂CO₃, and total reaction time was recorded. Samples were spun for 1 min at maximum speed (21,130 ***g***). Absorbance of the resulting supernatant was measured at 420 and 550 nm. The β-galactosidase activity was calculated using Eqn 1:

$$\text{Miller units} = \left\{ \frac{OD_{420} - 1.75 \times OD_{550}}{[t \times ((V_A/V_R) \times \quad OD_{600}]} \right\} \times 1000 \qquad (1)$$

where *t* is time, and V_A and V_R represent the actual volume assayed and the volume used to measure OD_{600}, respectively.

qPCR

Cells were grown to an early log phase overnight at 30°C. Tunicamycin was added to a final concentration of 2.5 μg/ml and incubated 1 h at 30°C or depleted of inositol for 2 h, when indicated. Total RNA was extracted using an RNeasy Mini Kit (Qiagen) following the manufacturer's protocol. DNase treatment in columns was carried out with RNase-free DNase (Qiagen, Venlo, Netherlands) following the manufacturer's protocol. cDNA was synthesized from 2 μg of total RNA using RevertAid reverse transcriptase (Thermo Fisher, Waltham, MA) following the manufacturer's protocol. SYBR Green qPCR experiments were performed following the manufacturer's protocol using a QuantStudio 6 Flex Real-time PCR system (Applied Biosystems, Waltham, MA). cDNA (30 ng) and 50 nM of paired primer mix was used for each reaction. Relative mRNA was determined with the comparative Ct method (ΔΔCt) normalized to housekeeping gene *ACT1*. Oligonucleotide primers used are listed in Table S3.

LD analysis

Cells were grown to early log phase, and 500 μl of the suspension was transferred on a coated slide with 10 mg/ml concanavalin A (Sigma-Aldrich, St Louis, MO) mounted onto an Attofluor cell chamber (Thermo Fisher, Waltham, MA) and imaged at room temperature. Tunicamycin was added to a final concentration of 2.5 μg/ml and incubated at 30°C for 1 h, when indicated. To stain LDs, cells were incubated with 0.05 μg/ml BODIPY 493/503 (Invitrogen) in phosphate-buffered saline (pH 7.4) for 10 min at room temperature, washed and resuspended in liquid medium before transferring into the Attofluor cell chamber for viewing. Samples were imaged with a Leica DMi8 system (HCX PL APO 100×/1.4–0.70 NA oil immersion objective) under the control of Metamorph ver. 7.8.10.0, or a Zeiss LSM710 microscope (100×1.4 NA Plan-Apochromat oil-immersion objective) under the control of Zen software (Carl Zeiss MicroImaging).

Genetic screen for temperature-sensitive alleles

The genetic screen was performed as previously reported (Thibault et al., 2011). A mutant library of the *SCS3* open reading frame flanked by 500 bp of its endogenous promoter and 300 bp of its terminator was generated by low-fidelity PCR using Taq DNA polymerase in the presence of 0.05 and 0.1 mM $MnCl_2$. DNA fragments were digested with *EcoRI* and *XbaI* and ligated into digested pRS316 to produce a plasmid library *scs3** with random point mutations. The strain YGT0492 was transformed with the mutant library pRS316-*scs3** and transformants were spread on selecting synthetic complete medium lacking uracil (SC −Ura) plates with limiting adenine (low Ade) at 6 µg/ml. Plates were incubated at 25°C until colonies developed fully red pigmentation due to low Ade. Colonies with a sectoring phenotype were streaked in duplicate on SC −Ura, low Ade, and incubated at 25°C and 37°C. For the primary screen, 123 colonies were screened for positive clones, which sectored at 25°C but remained red at 37°C. From the positive clones, the cells with a sectoring phenotype at 25°C were re-streaked in duplicate on SC-Ura, low Ade, and incubated at 25°C and 37°C to eliminate false positives. Positive clones were isolated without the plasmid pDN388. Plasmids were extracted from the clones and subjected to DNA sequencing analysis to identify the mutation present in the *scs3* temperature-sensitive (ts) alleles. The plasmid pGT0364, containing *scs3* ts allele (*scs3-1*) encodes for Scs3 with the following mutations D277G and I328V. The plasmid pGT0364 was transformed in strain YGT0492.

Lipid extraction and fatty acid analysis

Cells were grown to early log phase at 25°C followed by a 2 h incubation at 37°C. For whole-cell lipid extraction, 10 OD_{600} of cells was washed, pelleted in a glass vial and lyophilised using a Virtis freezer dryer under vacuum. All subsequent steps were carried out at 4°C. For lipid extraction of microsomes, 50 OD_{600} of cells was pelleted and resuspended in lysis buffer [50 mM Tris-HCl, pH 7.5, 150 mM NaCl, 5 mM EDTA, 1 mM PMSF and 1:200 dilution protease inhibitor cocktail (PIC, Sigma P8215)] and lysed mechanically by 15 times of 30 s interval using 0.5 mm zirconium beads at maximum speed of a vortex mixer. The supernatant was collected by spinning down the lysate 5 min at 800 *g*. The clarified lysate was spun down 1 h at 100,000 *g*. The pellet was resuspended in 100 µl ddH_2O and sonicated for 30 min before quantifying total protein using the bicinchoninic acid (BCA) protein quantification assay (Sigma-Aldrich). A volume corresponding to 0.5 mg of total protein (Klug and Daum, 2014) was transferred into glass vials and lyophilized using a Virtis freeze dryer under vacuum to record the dry weight of each sample. For lipid extraction from whole cells, samples were resuspended in 100 µl ddH_2O. Afterwards, 300 µl of 0.5 mm zirconium beads and 900 µl of chloroform ($CHCl_3$): methanol (2:1) were added before rigorous agitation of 2 h at 4°C. From here, 300 µl each of $CHCl_3$ and ddH_2O were added to the mixture and vortexed 15 s twice. The vials were centrifuged 6 min at 4250 *g*, and the lower organic phase was transferred to a new glass vial. The extraction step was repeated by the addition of 500 µl of $CHCl_3$ and further agitation for 2 h. Lipid extraction from microsomes was performed similarly with scaled-down reagent volumes. Combined extracts were concentrated, resuspended in 100 µl $CHCl_3$:methanol (2:1), and 30 µl was spotted on HPTLC Silica gel 60 plates (Merck Millipore) using Linomat 5 (CAMAG). Triacylglycerol (TAG) was separated with hexane:diethyl ether:acetic acid (75:25:2) and visualized under long-wave ultraviolet light (320 nm) by spraying 0.05 mg/ml of primuline dye in acetone:water (80:20) onto the dried plates.

Spots corresponding to TAG were scraped off the silica plates and transferred into glass vials. A total of 100 µl 1 mM pentadecanoic acid (C15:0) was added to the tubes as internal standard. TAGs were hydrolyzed and esterified to fatty acid methyl esters (FAME) with 300 µl of 1.25 M HCl-methanol for 1 h at 80°C. FAMEs were extracted three times with 1 ml of hexane. Combined extracts were dried under nitrogen, and resuspended in 20 µl of hexane. FAMEs were separated by gas chromatography with a flame ionisation detector (GC-FID; GC-2014, Shimadzu, Kyoto, Japan) using an ULBON HR-SS-10 50 m×0.25 mm column (Shinwa, Tokyo, Japan). Supelco 37 component FAME mix was used to identify corresponding FAs (Sigma-Aldrich, St Louis, MO). Data were normalized using the internal standard C15:0.

Transmission electron microscopy

Samples for transmission electron microscopy (TEM) were prepared as previously described (Wright, 2000). One OD_{600} unit of early log-phase cells grown at 25°C or 37°C was collected and pre-fixed with glutaraldehyde overnight at 4°C. Post-fixation was performed in the presence of 2% potassium permanganate for 1 h at room temperature. After dehydration in ethanol, cells were infiltrated with Spurr's resin and incubated for 24 h at 60°C to allow polymerization. Silver-gray sections were prepared using Ultracut UCT (Leica) equipped with a diamond knife and stained with lead citrate. Micrographs were taken using a transmission electron microscope (Joel JEM-1230).

Phospholipid analysis

Cells were grown to mid-log phase overnight in medium containing 75 µM inositol with (+cho) or without (−cho) 1 mM choline in the presence of 10 µCi/ml [^{32}P]orthophosphate. Cells collected by filtration were resuspended in medium with or without inositol or choline, as indicated, and in the presence of 10 µCi/ml [^{32}P]orthophosphate. Cells were harvested after 3 h following the shift or at indicated time point. Labeled lipids were extracted as previously described (Gaspar et al., 2006). The individual phospholipid species were resolved by two-dimensional thin layer chromatography. Phospholipids were separated using the solvent system chloroform:ethanol:water:triethylamine (30:35:7:35) for at least 2 h. Phospholipid identity was based on the mobility of known standards and quantified on a STORM 860 PhosphorImager (Amersham Biosciences).

Membrane yeast two-hybrid system screen

The bait plasmid for the expression of Scs3 and Yft2 fused with the Cub-LexA-VP16 reporter tag at either N- or C-terminus under the control of a TEF1 promoter was generated by cloning the respective coding sequences into the pTLB-1 or pTMBVα plasmid (Snider et al., 2010). Expression of the ScFIT bait proteins in the NMY51 reporter strain was verified with immunoblotting using anti-LexA antibodies (1:5000; Abcam ab50953) and anti-rabbit IgG IRDye 680 (1:15,000 dilution). Following verification of bait construct expression in the NMY51 reporter strain, the functionality of the reporter system was validated by co-expression of the bait construct with either a positive or negative control prey protein. Growth medium for bait constructs that activate the reporter with the negative control prey protein was adjusted for stringency using His3 competitor 3′-amino-1,2,4,-triazole (3-AT). The final concentrations of 3-AT supplemented to the growth medium, which yielded minimal self-activation, were 50 mM and 10 mM 3-AT for N-terminally tagged Scs3 and Yft2, respectively. The reporter strains bearing the bait constructs were then transformed with the NubG-X prey cDNA plasmid library (DualSystems), plated and incubated at 30°C until colonies appeared. Colonies were randomly selected and plated on selective plates supplemented with X-Gal for each screen. Plasmids from blue-colored colonies, indicative of positive bait–prey interaction, were recovered and amplified in DH5α competent bacteria cells. This was followed by plasmid extraction and sequencing. To reduce false-positive interactions, prey constructs were screened once more for specific interaction by retransformation back into yeast strains bearing the original bait protein. This was performed in comparison to a yeast strain expressing an unrelated negative control bait construct encoding for the human CD4 T-cell surface glycoprotein. Only prey constructs that exclusively activate the reporter with the bait construct of interest are included in the final list of interactors.

Cycloheximide chase assay

The cycloheximide chase assay was performed as previously described (Prasad et al., 2010). In brief, 6 OD_{600} units of early log phase cells were grown in appropriate selective medium. To induce lipid perturbation, 1 mM of choline chloride was added a day prior to harvesting, whereas inositol depletion was performed 2 h beforehand. Protein synthesis was inhibited by adding 200 µg/ml cycloheximide. Samples were taken at designated time points and trichloroacetic acid (TCA) was added to a final 10% volume. Cells were mechanically disrupted with 300 µl of 0.5 mm zirconium beads at 6500 rpm for 2×30 s using a tissue homogeniser (Precellys 24, Bertin Instruments). Precipitated proteins were pelleted 10 min at 21,000 *g*, 4°C, and resuspended in 40 µl of TCA resuspension buffer (100 mM Tris-HCl

pH 11, 3% SDS, 1 mM PMSF and PIC). Solubilized proteins were separated by SDS-PAGE, transferred on nitrocellulose membranes. Immunoblotting was performed with appropriate primary antibodies and IRDye-conjugated secondary antibodies. Proteins were visualized using the NIR fluorescence system (Odyssey CLx Imaging System). Values for each time point were normalized using anti-Tub1 as loading controls. Tonal quality was adjusted for representative images through ImageStudio Lite Version 5.2 (LI-COR Biosciences) where appropriate and was followed by quantification. All comparative analyses were performed on immunoblots performed in parallel using samples derived from the same experiment.

Global protein ubiquitylation assay

Strains expressing Myc-tagged ubiquitin (Ub–Myc) under the control of the inducible *CUP1* promoter were grown to early log phase. The culture medium was supplemented with a final concentration of 100 μM Cu_2SO_4, and cells were incubated for 3 h to allow Ub–Myc expression. Proteins were extracted from 2 OD_{600} units of cells and separated on SDS-acrylamide gels. Following transfer on nitrocellulose membranes, total protein on each lane was stained with REVERT Total Protein Stain (LI-COR Biosciences) followed by visualization on the Licor Odyssey CLx system. This was then followed by membrane blocking and incubation with antibodies against the Myc epitope tag (1:1000 dilution), and anti-mouse IgG IRDye 800 secondary antibodies (1:15,000). Total Myc-tagged protein signal was normalized against the total protein signal present as quantified through ImageStudio Lite Ver 5.2 (LI-COR Biosciences).

Statistics

Error bars indicate the s.e.m., calculated from at least three biological replicates, unless otherwise indicated. *P* values were calculated using one-way ANOVA with Tukey's post hoc test, unless otherwise indicated and reported as *P* values with four significant digits in the figures. All statistical tests were performed using GraphPad Prism 7 software.

Competing interests
The authors declare no competing or financial interests.

Author contributions
Conceptualization: G.T.; Methodology: W.S.Y., P.S., M.L.G., C.M., S.A.H., G.T.; Formal analysis: W.S.Y., P.S., M.L.G.; Validation: W.S.Y., P.S., M.L.G.; Investigation: W.S.Y., P.S., M.L.G., S.A.J., C.M.; Resources: W.S.Y., P.S., M.L.G.; Visualization: W.S.Y., P.S., G.T.; Writing - original draft: P.S., G.T.; Writing - review & editing: W.S.Y., M.L.G., G.T.; Supervision: G.T.; Project administration: G.T.; Funding acquisition: P.S., W.A.P., S.A.H., G.T.

Data availability
The original data for this study are available at the Dataverse Project doi:10.21979/N9/I7MXVP.

Supplementary information
Supplementary information available online at
https://jcs.biologists.org/lookup/doi/10.1242/jcs.248526.supplemental

Peer review history
The peer review history is available online at
https://jcs.biologists.org/lookup/doi/10.1242/jcs.248526.reviewer-comments.pdf

References

Adeyo, O., Horn, P. J., Lee, S. K., Binns, D. D., Chandrahas, A., Chapman, K. D. and Goodman, J. M. (2011). The yeast lipin orthologue Pah1p is important for biogenesis of lipid droplets. *J. Cell Biol.* **192**, 1043-1055. doi:10.1083/jcb.201010111

Allen, K. D., Chernova, T. A., Tennant, E. P., Wilkinson, K. D. and Chernoff, Y. O. (2007). Effects of ubiquitin system alterations on the formation and loss of a yeast prion. *J. Biol. Chem.* **282**, 3004-3013. doi:10.1074/jbc.M609597200

Becuwe, M., Bond, L. M., Pinto, A. F. M., Boland, S., Mejhert, N., Elliott, S. D., Cicconet, M., Graham, M. M., Liu, X. N., Ilkayeva, O. et al. (2020). FIT2 is an acyl–coenzyme A diphosphatase crucial for endoplasmic reticulum homeostasis. *J. Cell Biol.* **219**, e202006111. doi:10.1083/jcb.202006111

Cai, Y., McClinchie, E., Price, A., Nguyen, T. N., Gidda, S. K., Watt, S. C., Yurchenko, O., Park, S., Sturtevant, D., Mullen, R. T. et al. (2017). Mouse fat storage-inducing transmembrane protein 2 (FIT2) promotes lipid droplet accumulation in plants. *Plant Biotechnol. J.* **15**, 824-836. doi:10.1111/pbi.12678

Carman, G. M. and Henry, S. A. (1999). Phospholipid biosynthesis in the yeast Saccharomyces cerevisiae and interrelationship with other metabolic processes. *Prog. Lipid Res.* **38**, 361-399. doi:10.1016/S0163-7827(99)00010-7

Carman, G. M. and Kersting, M. C. (2004). Phospholipid synthesis in yeast: regulation by phosphorylation. *Biochem. Cell Biol.* **82**, 62-70. doi:10.1139/o03-064

Cartwright, B. R., Binns, D. D., Hilton, C. L., Han, S., Gao, Q. and Goodman, J. M. (2015). Seipin performs dissectible functions in promoting lipid droplet biogenesis and regulating droplet morphology. *Mol. Biol. Cell* **26**, 726-739. doi:10.1091/mbc.E14-08-1303

Chiabudini, M., Conz, C., Reckmann, F. and Rospert, S. (2012). Ribosome-associated complex and Ssb are required for translational repression induced by polylysine segments within nascent chains. *Mol. Cell. Biol.* **32**, 4769-4779. doi:10.1128/MCB.00809-12

Choudhary, V., Ojha, N., Golden, A. and Prinz, W. A. (2015). A conserved family of proteins facilitates nascent lipid droplet budding from the ER. *J. Cell Biol.* **211**, 261-271. doi:10.1083/jcb.201505067

Choudhary, V., Golani, G., Joshi, A. S., Cottier, S., Schneiter, R., Prinz, W. A. and Kozlov, M. M. (2018). Architecture of lipid droplets in endoplasmic reticulum is determined by phospholipid intrinsic curvature. *Curr. Biol.* **28**, 915-926.e9. doi:10.1016/j.cub.2018.02.020

Cox, J. S. and Walter, P. (1996). A novel mechanism for regulating activity of a transcription factor that controls the unfolded protein response. *Cell* **87**, 391-404. doi:10.1016/S0092-8674(00)81360-4

Cox, J. S., Chapman, R. E. and Walter, P. (1997). The unfolded protein response coordinates the production of endoplasmic reticulum protein and endoplasmic reticulum membrane. *Mol. Biol. Cell* **8**, 1805-1814. doi:10.1091/mbc.8.9.1805

Cretenet, G., Le Clech, M. and Gachon, F. (2010). Circadian clock-coordinated 12 hr period rhythmic activation of the IRE1alpha pathway controls lipid metabolism in mouse liver. *Cell Metab.* **11**, 47-57. doi:10.1016/j.cmet.2009.11.002

Estrada de Martin, P., Du, Y., Novick, P. and Ferro-Novick, S. (2005). Ice2p is important for the distribution and structure of the cortical ER network in Saccharomyces cerevisiae. *J. Cell Sci.* **118**, 65-77. doi:10.1242/jcs.01583

Fei, W., Wang, H., Fu, X., Bielby, C. and Yang, H. (2009). Conditions of endoplasmic reticulum stress stimulate lipid droplet formation in Saccharomyces cerevisiae. *Biochem. J.* **424**, 61-67. doi:10.1042/BJ20090785

Foresti, O., Ruggiano, A., Hannibal-Bach, H. K., Ejsing, C. S. and Carvalho, P. (2013). Sterol homeostasis requires regulated degradation of squalene monooxygenase by the ubiquitin ligase Doa10/Teb4. *eLife* **2**, e00953. doi:10.7554/eLife.00953

Fun, X. H. and Thibault, G. (2019). Lipid bilayer stress and proteotoxic stress-induced unfolded protein response deploy divergent transcriptional and non-transcriptional programmes. *Biochim. Biophys. Acta Mol. Cell Biol. Lipids* **1865**, 158449. doi:10.1016/j.bbalip.2019.04.009

Gaspar, M. L., Aregullin, M. A., Jesch, S. A. and Henry, S. A. (2006). Inositol induces a profound alteration in the pattern and rate of synthesis and turnover of membrane lipids in Saccharomyces cerevisiae. *J. Biol. Chem.* **281**, 22773-22785. doi:10.1074/jbc.M603548200

Grillitsch, K., Connerth, M., Köfeler, H., Arrey, T. N., Rietschel, B., Wagner, B., Karas, M. and Daum, G. (2011). Lipid particles/droplets of the yeast Saccharomyces cerevisiae revisited: lipidome meets proteome. *Biochim. Biophys. Acta* **1811**, 1165-1176. doi:10.1016/j.bbalip.2011.07.015

Gross, D. A., Snapp, E. L. and Silver, D. L. (2010). Structural insights into triglyceride storage mediated by fat storage-inducing transmembrane (FIT) protein 2. *PLoS ONE* **5**, e10796. doi:10.1371/journal.pone.0010796

Guan, X. L., Souza, C. M., Pichler, H., Dewhurst, G., Schaad, O., Kajiwara, K., Wakabayashi, H., Ivanova, T., Castillon, G. A., Piccolis, M. et al. (2009). Functional interactions between sphingolipids and sterols in biological membranes regulating cell physiology. *Mol. Biol. Cell* **20**, 2083-2095. doi:10.1091/mbc.e08-11-1126

Habeck, G., Ebner, F. A., Shimada-Kreft, H. and Kreft, S. G. (2015). The yeast ERAD-C ubiquitin ligase Doa10 recognizes an intramembrane degron. *J. Cell Biol.* **209**, 261-273. doi:10.1083/jcb.201408088

Halbleib, K., Pesek, K., Covino, R., Hofbauer, H. F., Wunnicke, D., Hanelt, I., Hummer, G. and Ernst, R. (2017). Activation of the unfolded protein response by lipid bilayer stress. Mol. Cell 67, 673-684.e8. doi:10.1016/j.molcel.2017.06.012

Hampton, R. Y., Gardner, R. G. and Rine, J. (1996). Role of 26S proteasome and HRD genes in the degradation of 3-hydroxy-3-methylglutaryl-CoA reductase, an integral endoplasmic reticulum membrane protein. Mol. Biol. Cell 7, 2029-2044. doi:10.1091/mbc.7.12.2029

Hayes, M. J., Choudhary, V., Ojha, N., Shin, J. J. H., Han, G.-S., Carman, G. M., Loewen, C. J. R., Prinz, W. A. and Levine, T. (2017). Fat storage-inducing transmembrane (FIT or FITM) proteins are related to lipid phosphatase/phosphotransferase enzymes. Microb. Cell 5, 88-103. doi:10.15698/mic2018.02.614

Henry, S. A. and Patton-Vogt, J. L. (1998). Genetic regulation of phospholipid metabolism: yeast as a model eukaryote. Prog. Nucleic Acid Res. Mol. Biol. 61, 133-179. doi:10.1016/S0079-6603(08)60826-0

Henry, S. A., Kohlwein, S. D. and Carman, G. M. (2012). Metabolism and regulation of glycerolipids in the yeast Saccharomyces cerevisiae. Genetics 190, 317-349. doi:10.1534/genetics.111.130286

Ho, N., Yap, W. S., Xu, J., Wu, H., Koh, J. H., Goh, W. W. B., George, B., Chong, S. C., Taubert, S. and Thibault, G. (2020). Stress sensor Ire1 deploys a divergent transcriptional program in response to lipid bilayer stress. J. Cell Biol. 219, e201909165. doi:10.1083/jcb201909165

Hosaka, K., Nikawa, J.-I., Kodaki, T., Ishizu, H. and Yamashita, S. (1994). Cloning and sequence of the SCS3 gene which is required for inositol prototrophy in Saccharomyces cerevisiae. J. Biochem. 116, 1317-1321. doi:10.1093/oxfordjournals.jbchem.a124681

Hou, N. S., Gutschmidt, A., Choi, D. Y., Pather, K., Shi, X., Watts, J. L., Hoppe, T. and Taubert, S. (2014). Activation of the endoplasmic reticulum unfolded protein response by lipid disequilibrium without disturbed proteostasis in vivo. Proc. Natl. Acad. Sci. USA 111, E2271-E2280. doi:10.1073/pnas.1318262111

Hsieh, L.-S., Su, W.-M., Han, G.-S. and Carman, G. M. (2015). Phosphorylation regulates the ubiquitin-independent degradation of yeast Pah1 phosphatidate phosphatase by the 20S proteasome. J. Biol. Chem. 290, 11467-11478. doi:10.1074/jbc.M115.648659

Ishii, A., Kawai, M., Noda, H., Kato, H., Takeda, K., Asakawa, K., Ichikawa, Y., Sasanami, T., Tanaka, K. and Kimura, Y. (2018). Accelerated invagination of vacuoles as a stress response in chronically heat-stressed yeasts. Sci. Rep. 8, 2644. doi:10.1038/s41598-018-20781-8

Jacquier, N., Choudhary, V., Mari, M., Toulmay, A., Reggiori, F. and Schneiter, R. (2011). Lipid droplets are functionally connected to the endoplasmic reticulum in Saccharomyces cerevisiae. J. Cell Sci. 124, 2424-2437. doi:10.1242/jcs.076836

Jonikas, M. C., Collins, S. R., Denic, V., Oh, E., Quan, E. M., Schmid, V., Weibezahn, J., Schwappach, B., Walter, P., Weissman, J. S. et al. (2009). Comprehensive characterization of genes required for protein folding in the endoplasmic reticulum. Science 323, 1693-1697. doi:10.1126/science.1167983

Kadereit, B., Kumar, P., Wang, W.-J., Miranda, D., Snapp, E. L., Severina, N., Torregroza, I., Evans, T. and Silver, D. L. (2008). Evolutionarily conserved gene family important for fat storage. Proc. Natl. Acad. Sci. USA 105, 94-99. doi:10.1073/pnas.0708579105

Kandasamy, P., Vemula, M., Oh, C.-S., Chellappa, R. and Martin, C. E. (2004). Regulation of unsaturated fatty acid biosynthesis in Saccharomyces: the endoplasmic reticulum membrane protein, Mga2p, a transcription activator of the OLE1 gene, regulates the stability of the OLE1 mRNA through exosome-mediated mechanisms. J. Biol. Chem. 279, 36586-36592. doi:10.1074/jbc.M401557200

Kanehara, K., Xie, W. and Ng, D. T. W. (2010). Modularity of the Hrd1 ERAD complex underlies its diverse client range. J. Cell Biol. 188, 707-716. doi:10.1083/jcb.200907055

Klug, L. and Daum, G. (2014). Yeast lipid metabolism at a glance. FEMS Yeast Res. 14, 369-388. doi:10.1111/1567-1364.12141

Kory, N., Farese, R. V., Jr. and Walther, T. C. (2016). Targeting fat: mechanisms of protein localization to lipid droplets. Trends Cell Biol. 26, 535-546. doi:10.1016/j.tcb.2016.02.007

Lee, A.-H., Scapa, E. F., Cohen, D. E. and Glimcher, L. H. (2008). Regulation of hepatic lipogenesis by the transcription factor XBP1. Science 320, 1492-1496. doi:10.1126/science.1158042

Lee, J. S., Mendez, R., Heng, H. H., Yang, Z. Q. and Zhang, K. (2012). Pharmacological ER stress promotes hepatic lipogenesis and lipid droplet formation. Am. J. Transl. Res. 4, 102-113.

Lee, S.-J., Zhang, J., Choi, A. M. K. and Kim, H. P. (2013). Mitochondrial dysfunction induces formation of lipid droplets as a generalized response to stress. Oxid. Med. Cell Longev. 2013, 327167. doi:10.1155/2013/327167

Liu, M., Huang, C., Polu, S. R., Schneiter, R. and Chang, A. (2012). Regulation of sphingolipid synthesis through Orm1 and Orm2 in yeast. J. Cell Sci. 125, 2428-2435. doi:10.1242/jcs.100578

Liu, L., Zhang, K., Sandoval, H., Yamamoto, S., Jaiswal, M., Sanz, E., Li, Z., Hui, J., Graham, B. H. and Quintana, A. (2015). Glial lipid droplets and ROS induced by mitochondrial defects promote neurodegeneration. Cell 160, 177-190. doi:10.1016/j.cell.2014.12.019

Loewen, C. J. R., Young, B. P., Tavassoli, S. and Levine, T. P. (2007). Inheritance of cortical ER in yeast is required for normal septin organization. J. Cell Biol. 179, 467-483. doi:10.1083/jcb.200708205

Markgraf, D. F., Klemm, R. W., Junker, M., Hannibal-Bach, H. K., Ejsing, C. S. and Rapoport, T. A. (2014). An ER protein functionally couples neutral lipid metabolism on lipid droplets to membrane lipid synthesis in the ER. Cell Rep. 6, 44-55. doi:10.1016/j.celrep.2013.11.046

Moir, R. D., Gross, D. A., Silver, D. L. and Willis, I. M. (2012). SCS3 and YFT2 link transcription of phospholipid biosynthetic genes to ER stress and the UPR. PLoS Genet. 8, e1002890. doi:10.1371/journal.pgen.1002890

Natter, K. and Kohlwein, S. D. (2013). Yeast and cancer cells - common principles in lipid metabolism. Biochim. Biophys. Acta 1831, 314-326. doi:10.1016/j.bbalip.2012.09.003

Nguyen, L. N., Hamari, Z., Kadereit, B., Trofa, D., Agovino, M., Martinez, L. R., Gacser, A., Silver, D. L. and Nosanchuk, J. D. (2011). Candida parapsilosis fat storage-inducing transmembrane (FIT) protein 2 regulates lipid droplet formation and impacts virulence. Microbes Infect. 13, 663-672. doi:10.1016/j.micinf.2011.02.009

Nguyen, T. B., Louie, S. M., Daniele, J. R., Tran, Q., Dillin, A., Zoncu, R., Nomura, D. K. and Olzmann, J. A. (2017). DGAT1-dependent lipid droplet biogenesis protects mitochondrial function during starvation-induced autophagy. Dev. Cell 42, 9-21.e5. doi:10.1016/j.devcel.2017.06.003

Ohba, M. (1994). A 70-kDa heat shock cognate protein suppresses the defects caused by a proteasome mutation in Saccharomyces cerevisiae. FEBS Lett. 351, 263-266. doi:10.1016/0014-5793(94)00873-6

Olzmann, J. A., Richter, C. M. and Kopito, R. R. (2013). Spatial regulation of UBXD8 and p97/VCP controls ATGL-mediated lipid droplet turnover. Proc. Natl. Acad. Sci. USA 110, 1345-1350. doi:10.1073/pnas.1213738110

Pascual, F., Hsieh, L.-S., Soto-Cardalda, A. and Carman, G. M. (2014). Yeast Pah1p phosphatidate phosphatase is regulated by proteasome-mediated degradation. J. Biol. Chem. 289, 9811-9822. doi:10.1074/jbc.M114.550103

Prasad, R., Kawaguchi, S. and Ng, D. T. W. (2010). A nucleus-based quality control mechanism for cytosolic proteins. Mol. Biol. Cell 21, 2117-2127. doi:10.1091/mbc.e10-02-0111

Quon, E., Sere, Y. Y., Chauhan, N., Johansen, J., Sullivan, D. P., Dittman, J. S., Rice, W. J., Chan, R. B., Di Paolo, G., Beh, C. T. et al. (2018). Endoplasmic reticulum-plasma membrane contact sites integrate sterol and phospholipid regulation. PLoS Biol. 16, e2003864. doi:10.1371/journal.pbio.2003864

Ramus, S. J., Kartsonaki, C., Gayther, S. A., Pharoah, P. D. P., Sinilnikova, O. M., Beesley, J., Chen, X., McGuffog, L., Healey, S., Couch, F. J. et al. (2011). Genetic variation at 9p22.2 and ovarian cancer risk for BRCA1 and BRCA2 mutation carriers. J. Natl. Cancer Inst. 103, 105-116. doi:10.1093/jnci/djq494

Ravid, T., Kreft, S. G. and Hochstrasser, M. (2006). Membrane and soluble substrates of the Doa10 ubiquitin ligase are degraded by distinct pathways. EMBO J. 25, 533-543. doi:10.1038/sj.emboj.7600946

Ruggiano, A., Mora, G., Buxó, L. and Carvalho, P. (2016). Spatial control of lipid droplet proteins by the ERAD ubiquitin ligase Doa10. EMBO J. 35, 1644-1655. doi:10.15252/embj.201593106

Schuldiner, M., Collins, S. R., Thompson, N. J., Denic, V., Bhamidipati, A., Punna, T., Ihmels, J., Andrews, B., Boone, C., Greenblatt, J. F. et al. (2005). Exploration of the function and organization of the yeast early secretory pathway through an epistatic miniarray profile. Cell 123, 507-519. doi:10.1016/j.cell.2005.08.031

Selvaraju, K., Rajakumar, S. and Nachiappan, V. (2014). Identification of a phospholipase B encoded by the LPL1 gene in Saccharomyces cerevisiae. Biochim. Biophys. Acta 1841, 1383-1392. doi:10.1016/j.bbalip.2014.06.013

Shcherbik, N. and Haines, D. S. (2007). Cdc48p(Npl4p/Ufd1p) binds and segregates membrane-anchored/tethered complexes via a polyubiquitin signal present on the anchors. Mol. Cell 25, 385-397. doi:10.1016/j.molcel.2007.01.024

Shyu, P., Jr, Ng, B. S. H., Ho, N., Chaw, R., Seah, Y. L., Marvalim, C. and Thibault, G. (2019). Membrane phospholipid alteration causes chronic ER stress through early degradation of homeostatic ER-resident proteins. Sci. Rep. 9, 8637. doi:10.1038/s41598-019-45020-6

Snider, J., Kittanakom, S., Damjanovic, D., Curak, J., Wong, V. and Stagljar, I. (2010). Detecting interactions with membrane proteins using a membrane two-hybrid assay in yeast. Nat. Protoc. 5, 1281-1293. doi:10.1038/nprot.2010.83

Spear, E. D. and Ng, D. T. W. (2003). Stress tolerance of misfolded carboxypeptidase Y requires maintenance of protein trafficking and degradative pathways. Mol. Biol. Cell 14, 2756-2767. doi:10.1091/mbc.e02-11-0717

Stordeur, C., Puth, K., Sáenz, J. P. and Ernst, R. (2014). Crosstalk of lipid and protein homeostasis to maintain membrane function. Biol. Chem. 395, 313-326. doi:10.1515/hsz-2013-0235

Surma, M. A., Klose, C., Peng, D., Shales, M., Mrejen, C., Stefanko, A., Braberg, H., Gordon, D. E., Vorkel, D., Ejsing, C. S. et al. (2013). A lipid E-MAP identifies Ubx2 as a critical regulator of lipid saturation and lipid bilayer stress. Mol. Cell 51, 519-530. doi:10.1016/j.molcel.2013.06.014

Swanson, R., Locher, M. and Hochstrasser, M. (2001). A conserved ubiquitin ligase of the nuclear envelope/endoplasmic reticulum that functions in both ER-associated and Matalpha2 repressor degradation. Genes Dev. 15, 2660-2674. doi:10.1101/gad.933301

Szymanski, K. M., Binns, D., Bartz, R., Grishin, N. V., Li, W.-P., Agarwal, A. K., Garg, A., Anderson, R. G. W. and Goodman, J. M. (2007). The lipodystrophy protein seipin is found at endoplasmic reticulum lipid droplet junctions and is important for droplet morphology. *Proc. Natl. Acad. Sci. USA* **104**, 20890-20895. doi:10.1073/pnas.0704154104

Tavassoli, S., Chao, J. T., Young, B. P., Cox, R. C., Prinz, W. A., de Kroon, A. I. P. M. and Loewen, C. J. (2013). Plasma membrane–endoplasmic reticulum contact sites regulate phosphatidylcholine synthesis. *EMBO Rep.* **14**, 434-440. doi:10.1038/embor.2013.36

Thibault, G. and Ng, D. T. W. (2011). A screen for mutants requiring activation of the unfolded protein response for viability. *Methods Enzymol.* **491**, 199-216. doi:10.1016/B978-0-12-385928-0.00012-2

Thibault, G., Ismail, N. and Ng, D. T. W. (2011). The unfolded protein response supports cellular robustness as a broad-spectrum compensatory pathway. *Proc. Natl. Acad. Sci. USA* **108**, 20597-20602. doi:10.1073/pnas.1117184109

Thibault, G., Shui, G., Kim, W., McAlister, G. C., Ismail, N., Gygi, S. P., Wenk, M. R. and Ng, D. T. W. (2012). The membrane stress response buffers lethal effects of lipid disequilibrium by reprogramming the protein homeostasis network. *Mol. Cell* **48**, 16-27. doi:10.1016/j.molcel.2012.08.016

To, M., Peterson, C. W. H., Roberts, M. A., Counihan, J. L., Wu, T. T., Forster, M. S., Nomura, D. K. and Olzmann, J. A. (2017). Lipid disequilibrium disrupts ER proteostasis by impairing ERAD substrate glycan trimming and dislocation. *Mol. Biol. Cell* **28**, 270-284. doi:10.1091/mbc.e16-07-0483

Travers, K. J., Patil, C. K., Wodicka, L., Lockhart, D. J., Weissman, J. S. and Walter, P. (2000). Functional and genomic analyses reveal an essential coordination between the unfolded protein response and ER-associated degradation. *Cell* **101**, 249-258. doi:10.1016/S0092-8674(00)80835-1

van Meer, G., Voelker, D. R. and Feigenson, G. W. (2008). Membrane lipids: where they are and how they behave. *Nat. Rev. Mol. Cell Biol.* **9**, 112-124. doi:10.1038/nrm2330

Wang, S. and Kaufman, R. J. (2012). The impact of the unfolded protein response on human disease. *J. Cell Biol.* **197**, 857-867. doi:10.1083/jcb.201110131

Weisshaar, N., Welsch, H., Guerra-Moreno, A. and Hanna, J. (2017). Phospholipase Lpl1 links lipid droplet function with quality control protein degradation. *Mol. Biol. Cell* **28**, 716-725. doi:10.1091/mbc.e16-10-0717

Wright, R. (2000). Transmission electron microscopy of yeast. *Microsc. Res. Tech.* **51**, 496-510. doi:10.1002/1097-0029(20001215)51:6<496::AID-JEMT2>3.0.CO;2-9